Characterization of Horizontal Lipid Bilayers as a Model System to Study Lipid Phase Separation

Alf Honigmann,[†] Claudius Walter,[‡] Frank Erdmann,[†] Christian Eggeling,[§] and Richard Wagner[†*]
[†]Universität Osnabrück, Fachbereich Biologie/Chemie, Osnabrück, Germany; [‡]Ionovation GmbH, Osnabrück, Germany; and [§]Max-Planck-Institut für Biophysikalische Chemie, Abteilung NanoBiophotonik, Göttingen, Germany

ABSTRACT Artificial lipid membranes are widely used as a model system to study single ion channel activity using electrophysiological techniques. In this study, we characterize the properties of the artificial bilayer system with respect to its dynamics of lipid phase separation using single-molecule fluorescence fluctuation and electrophysiological techniques. We determined the rotational motions of fluorescently labeled lipids on the nanosecond timescale using confocal time-resolved anisotropy to probe the microscopic viscosity of the membrane. Simultaneously, long-range mobility was investigated by the lateral diffusion of the lipids using fluorescence correlation spectroscopy. Depending on the solvent used for membrane preparation, lateral diffusion coefficients in the range $D_{lat} = 10–25\ \mu m^2/s$ and rotational diffusion coefficients ranging from $D_{rot} = 2.8 - 1.4 \times 10^7\ s^{-1}$ were measured in pure liquid-disordered (L_d) membranes. In ternary mixtures containing saturated and unsaturated phospholipids and cholesterol, liquid-ordered (L_o) domains segregated from the L_d phase at 23°C. The lateral mobility of lipids in L_o domains was around eightfold lower compared to those in the L_d phase, whereas the rotational mobility decreased by a factor of 1.5. Burst-integrated steady-state anisotropy histograms, as well as anisotropy imaging, were used to visualize the rotational mobility of lipid probes in phase-separated bilayers. These experiments and fluorescence correlation spectroscopy measurements at different focal diameters indicated a heterogeneous microenvironment in the L_o phase. Finally, we demonstrate the potential of the opto-electro setup to study the influence of lipid domains on the electrophysiological properties of ion channels. We found that the electrophysiological activity of gramicidin A (gA), a well-characterized ion-channel-forming peptide, was related to lipid-domain partitioning. During liquid-liquid phase separation, gA was largely excluded from L_o domains. Simultaneously, the number of electrically active gA dimers increased due to the increased surface density of gA in the L_d phase.

INTRODUCTION

The lipid composition of biological membranes, along with its spatial organization and temporal dynamics, are acknowledged increasingly to be fundamental to the function and regulation of integral and membrane-associated proteins (1,2). Data obtained by various labs using different techniques provide growing evidence that cell membranes are organized in separated, spatially confined, and dynamic domains (3–11). Many details of these domains, such as their molecular characteristics and their size distribution, which is somewhere below the resolution limit of conventional light microscopy, remain to be clarified. Two fundamental determinants for the origin of membrane compartmentalization have been found. First, the lateral mobility in a cell membrane seems to be bounded by protein/lipid interactions with the cytoskeleton meshwork. Second, phase separation of lipid components and cholesterol into liquid-ordered (L_o) and liquid-disordered (L_d) domains may cause sorting of membrane components according to their affinity for different lipid phases.

The nature of lipid phase separation has been studied in detail using model membranes like giant unilamellar vesicles and supported lipid bilayers (12–17). The biologically interesting regimes where L_o and L_d phases coexist have been mapped in phase diagrams (13,18–21). To study the dynamics of lipids and proteins in coexisting L_o and L_d phases, techniques such as fluorescence recovery after photobleaching, fluorescence resonance energy transfer, single-particle tracking, and fluorescence correlation spectroscopy (FCS) have been employed. In this context, FCS (22,23) and its recent advancements (7,11,24,25) have been proven to be a particularly valuable tool. Using FCS, the concentration and lateral diffusion of single dye-labeled (lipid and proteins) probes can be evaluated with high statistical accuracy. In addition, free versus hindered diffusion can be discriminated at the nanometer scale (7,11). Another fluorescence method that is sensitive to the dynamics of lipid probes is time-resolved anisotropy (TRA) (26,27). However, in contrast to FCS, which detects lateral movements in the microsecond-to-millisecond range, TRA is used to measure rotational dynamics occurring during the fluorescence lifetime of the probe. The rotational correlation times and the limiting anisotropy of lipid probes revealed by TRA report the short-range interactions within the very local environment of the studied probe, which can be related to the order of the acyl chains of lipids (28,29).

One key function of a biological membrane is its electrical excitability, which is the basis of signaling, as well as energy-conserving, processes in cells (30). However, most of the model systems used to study lipid phase separation

Submitted November 3, 2009, and accepted for publication March 15, 2010.

*Correspondence: wagner@uos.de

F. Erdmann's present address is Universität Münster, Institut für Physiologie I, Robert-Koch-Str. 27a, 48149 Münster, Germany.

Editor: Lukas K. Tamm.

0006-3495/10/06/2886/9 $2.00

doi: 10.1016/j.bpj.2010.03.033

processes lack a controlled accession of this important parameter of a lipid membrane. In this study, we used electrically addressable, horizontal planar bilayers separating two water bulk phases, also referred to as black lipid membranes (BLMs), in combination with a polarization-sensitive FCS setup. The setup permits electrical recordings simultaneous with evaluation of the lateral (FCS) and rotational diffusion (TRA) of fluorescently labeled probes. BLMs have been employed traditionally in electrophysiology to record single-channel currents of purified reconstituted membrane proteins (31–33), but they have also been used in combination with fluorescence microscopy and FCS (34–36). However, to our knowledge, BLMs have been used in only one study as a model system to analyze lipid phase separation. Samsonov et al. showed qualitatively that large-scale L_o and L_d domains coexist in BLMs when ternary lipid compositions are cooled below the phase transition temperature (T_m) (37). The BLMs bear some advantages over other model systems, such as supported lipid bilayers. First, the lipid phase separation is not disturbed by any surface interaction. Second, this system allows for an easy exchange of the surrounding solution. Finally, the optoelectrical setup permits the application of membrane potentials and measurement of the according membrane currents.

Here, we characterize horizontal BLMs with respect to temperature-dependent dynamics of lipid motion and domain formation at the single-molecule level. As a test case for electrooptical measurements, we use fluorescently labeled gramicidin A (gA), a simple and well-characterized peptide ion channel (36,38).

MATERIALS AND METHODS

Chemicals

2-Dioleoyl-*sn*-glycero-3-phosphocholine (DOPC) was purchased from Avanti Polar Lipids (Alabaster, AL). Distereoyl-*sn*-glycero-3-phosphocoline (DSPC), cholesterol (CO), *n*-decane, *n*-hexane, squalene, and gramicidin A were purchased from Sigma Aldrich (Munich, Germany). Cholesteryl-BODIPY FL C_{12} (CO-BDY) was purchased from Molecular Probes (Eugene, OR). The organic dye Atto647N (fluorescence excitation and emission maxima of 645 and 670 nm, respectively; Atto-Tec, Siegen, Germany)-labeled phosphoethanolamine lipid Atto647N-1,2-dihexdecanoyl-*sn*-glycero-3-phosphatidyl-ethanolamine (DPPE647), the Atto647N-labeled sphingomyelin lipid Atto647N-sphingomyelin (SM647), and the Atto647N-labeled Atto647N-ceramide (CER647) were prepared by Atto-Tec and were previously applied in live-cell studies. The structures of Atto647N and the labeled lipids are depicted in the supplement of Eggeling et al. (11). Although DPPE647 is labeled at the headgroup, i.e., in the water phase, SM647 and CER647 are labeled at the water-lipid interface by replacing the native long acyl chain with a short acyl chain carrying the dye.

Lipids were stored in methanol/chloroform (1:1) under nitrogen at −20°C. For bilayer preparation, lipids were mixed accordingly, dried under vacuum, and dissolved in hydrocarbons to a final concentration of 50 mg/ml. To yield an appropriate label concentration in the bilayer for fluorescence fluctuation analysis, the lipids/labeled lipids molar ratio was adjusted to 50,000:1.

Horizontal lipid bilayers

The horizontal bilayer chip is made of polytetrafluoroethylene (PTFE) with drilled holes for *cis* and *trans* compartments and electrode access. A 25-μm thin PTFE sheet with a round ~100-μm small aperture is sandwiched between a coverslide and the chamber body using double-sided adhesive film (Fig. 1 *A*). The lower adhesive film contains a laser-edged channel structure to connect the *trans* compartments (Fig. 1 *B*). The exclusive connection between the *cis* and *trans* compartment is the aperture in the PTFE sheet. The bilayer was painted over the aperture using a 90° bent Hamilton syringe (Bonaduz, Switzerland). Bilayer formation was monitored optically and electrically. The distance between the coverslide and the planar bilayer is 100 μm, which allows optical access by high-numerical-aperture water objectives required for fluorescence fluctuation analysis (Fig. 1 *A*). For electrical measurements, silver/silver chloride electrodes embedded in agarose were connected to the *cis* and *trans* compartments. Electrical recordings were made using a CV-5-1GU headstage connected to a GeneClamp 500B amplifier from Axon Instruments (Sunnyvale, CA). Data were digitalized with a Digidata 1322A and monitored with the software Clampex 9 (Axon Instruments, Union City, CA). After each measurement session, the coverslide with the adhesives was removed and the chamber body was cleaned in ethanol before reuse. Disposable chips are meanwhile commercially available (Ionovation GmbH, Osnabrück, Germany).

For preparation of pure L_d bilayers, DOPC was used as the only lipid component. Ternary mixtures of DOPC/DSPC/CO in a molar ratio of 2-1:1:1 were used for phase separation studies, according to the phase diagram in Feigenson (20).

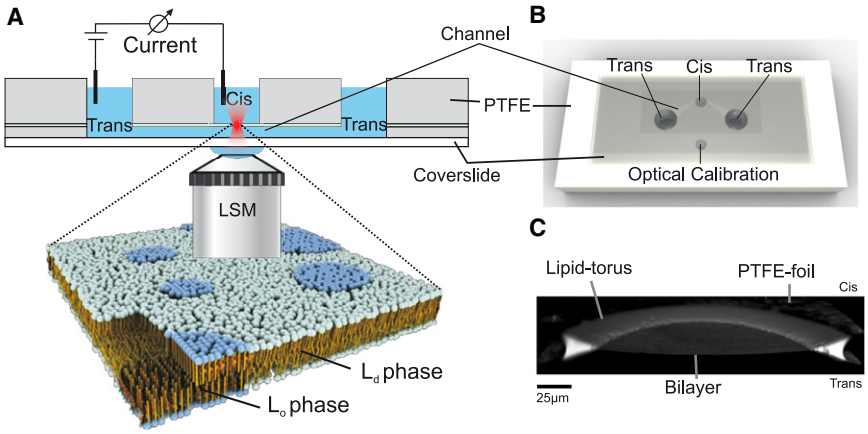

FIGURE 1 Setup of the horizontal bilayer chamber. (*A*) Schematic view of the setup. The chamber contains two compartments (*cis* and *trans*) separated by a thin PTFE film. The film is perforated by a 100-μm hole, which is the only connection between the *trans* and *cis* compartments. When a lipid solution is painted over the hole, a bilayer forms spontaneously. The membrane is accessible by a high-numerical-aperture water objective. Electrodes in *cis* and *trans* allow electrophysiological recordings of the bilayer. (*B*) Bottom view of the chamber. The *cis* and *trans* compartments have a buffer volume of 100 μl. (*C*) Side-cut of a three-dimensional reconstruction (LSM *YZ*-stack) of the bilayer. The membrane spans the aperture in the PTFE film. The interface of the film and the bilayer is bridged by the torus, which contains the bulk solvent and lipids.

Confocal microscopy

Confocal imaging and fluorescence fluctuation recordings were performed on an Insight Cell 3D microscope from Evotec technologies (Hamburg, Germany, now Perkin Elmer), equipped with a 543-nm continuous-wave HeNe and a 635-nm pulsed diode laser (~80-ps pulse width; PicoQuant, Berlin, Germany), a 40× water immersion objective (UApo340 40×, NA 1.15, Olympus, Tokyo, Japan), and avalanche photodiode detectors (SPCM-AQR-13-FC; Perkin Elmer Optoelectronics, Fremont, CA). Fluorescence excitation was performed with linear polarized light, and the laser power was adjusted to 5–20 μW. The emission light was split according to polarization and detected on two channels, each equipped with a detector. The signal from each detector was split up on the correlator and the imaging unit of the Insight and on a PHR 800 router in combination with a PicoHarp 300 counting module (PicoQuant). The PicoHarp 300 allowed for an interactive analysis such as the recording of raw photon traces and online FCS and lifetime analysis. The repetition rate of the laser was set to 40 MHz and the resolution of the PicoHarp 300 to 16 ps.

For z-scan measurements, the focus was moved in the Z-direction in 100-nm steps through the membrane and 20-s photon traces were recorded at each position. If the count rate was stable over the measurement period, the traces were analyzed to determine rotational (TRA) and lateral (FCS) diffusion times using the software SymphoTime and FluoFit (PicoQuant).

Time-resolved anisotropy

Rotational diffusion times were evaluated by globally fitting the parallel, $I_{\|}$, and perpendicular, $I_{\perp}$, fluorescence decay according to the Eggeling et al. model (39):

$$I_{\|}(t) = G\int_{-\infty}^{t} IRF_{\|}(t')\frac{1}{3}\,\alpha e^{-\frac{t-t'}{\tau_{FL}}}\left[1 + 2\left(R_{INF} + \beta e^{\frac{t-t'}{\phi}}\right)\right]dt', \tag{1}$$

$$I_{\perp}(t) = G\int_{-\infty}^{t} IRF_{\perp}(t')\frac{1}{3}\alpha e^{-\frac{t-t'}{\tau_{FL}}}\left[1 - \left(R_{INF} + \beta e^{\frac{t-t'}{\phi}}\right)\right]dt', \tag{2}$$

where G accounts for the different detection sensitivities in the two detection channels, $IRF_{\|}(t)$ and $IRF_{\perp}(t)$ are the time-resolved instrument response functions of the microscope, τ_{FL} and α are the characteristic decay time (fluorescence lifetime) and amplitude, respectively, of the fluorescence lifetime component, R_{INF} is the residual anisotropy (for $t \rightarrow \infty$), and Φ and β are the characteristic decay time (rotational correlation time) and the initial anisotropy, respectively. The value of $G = 0.95$ was determined by tail-matching the parallel and vertically polarized decays of a fast-rotating dye (Atto647N in aqueous buffer). The instrument response function (IRF) of the microscope was recorded using reflected laser light at the coverslip interface. R_{INF} was zero in all of our fits. Depolarization due to the focusing optics has not been corrected for in this model. The goodness of fit was judged by χ^2 (1–1.5) and the residuals. The rotational diffusion coefficient was calculated according to $D_{\mathrm{rot}} = 1/(6\Phi)$.

Fluorescence correlation spectroscopy

The translational diffusion time, τ_D, was evaluated using cross-correlation between the parallel and perpendicular polarized photon traces. The correlation curves were fitted by a two-dimensional diffusion model including a triplet term (40):

$$G(\tau) = \frac{1}{N}\frac{1}{\left(1 + t/\tau_D\right)}\left(1 + \frac{T}{1-T}\,e^{\frac{-t}{\tau_T}}\right), \tag{3}$$

where N is the mean number of particles in the confocal volume. T is the average fraction of molecules that are in the triplet state, and τ_T the triplet correlation time, which depends on the sum of the population and depopulation rates of the triplet system. $\tau_D = {w_0}^2/(4D_{\mathrm{lat}})$ is the average molecular diffusion time through the Gaussian-assumed focal intensity profile and is characterized by the lateral diffusion coefficients, D_{lat}, and the focal radius, w_0 (defined as the radius at which the Gaussian-assumed focal intensity profile has dropped to $1/e^2$ of its maximum value). w_0 was estimated from FCS measurements on the dye Atto655-maleimid in aqueous buffer with the known diffusion coefficient $D_{\mathrm{lat}} = 407\ \mu\mathrm{m}^2/\mathrm{s}$ (41). A good estimate of the lateral lipid membrane mobility, D_{lat} was obtained from the shortest diffusion time, τ_D, determined for the correlation curves recorded from a z-scan over the bilayer.

More exact values of D_{lat} and w_0 were determined by using z-scan FCS (42). The diffusion times $\tau_D(\Delta z)$ determined from correlation data recorded at different z-positions, Δz, of the focus relative to the BLM were fitted to

$$\tau_D = \frac{w_0^2}{4D_{\mathrm{lat}}}\left(1 + \frac{\lambda^2\Delta Z^2}{\pi^2 n^2 w_0^4}\right), \tag{4}$$

where λ is the excitation wavelength and n the refractive index of the buffer.

Steady-state anisotropy

The steady-state anisotropy, r, was calculated from the average signal count rates, $I_{\|}$, and $I_{\perp}$, in the parallel and perpendicular detection channels, respectively, and from the G-factor defined in Eqs. 1 and 2.

$$\bar{r} = \frac{I_{\|} - GI_{\perp}}{I_{\|} + 2GI_{\perp}}. \tag{5}$$

Scanning anisotropy images were calculated pixelwise using Eq. 5 with the software ImageJ (http://rsbweb.nih.gov/ij/), or the steady-state anisotropy, r, was determined at the single-molecule level (43). To achieve this, photon traces recorded for a very diluted sample (far less than one fluorescent molecule per laser spot) were binned at 1-ms resolution, fluorescence bursts due to single-molecule transits were selected by introducing a threshold to distinguish the photon burst from background, and the single-molecule steady-state anisotropy was calculated from all the photons selected from a single burst using the software SymphoTime from PicoQuant.

Gramicidin A labeling and electrophysiological activity

C-terminal labeling of gA with Atto637-NHS (Atto-Tec, Siegen, Germany) was conducted as described in Borisenko et al. (36). Briefly, a primary amino group was added to the peptide by coupling ethylenediamine to the hydroxyl group of the C-terminus. In a second reaction, the NHS-ester group of Atto637 reacted with the primary amine to result in the product gA-637. The labeled peptide was purified from excess dye by dilution with water and subsequent centrifugation. The hydrophobic peptide was recovered in the pellet. This procedure was repeated until no free dye was detectable in the supernatant. Finally, the pellet was dissolved in methanol and the solution was stored at −20°C. The degree of labeling determined by spectroscopy (A_{280} and A_{637}) was 0.5. The mean single-channel conductance values for unmodified gA and gA-637 were ~18 pS in a DOPC bilayer suspended in 1 M NaCl.

The dimerization constant of gA-637 was determined according to (44)

$$K = \frac{G_2}{4G_2^2 - 4G_2 * G_0 + G_0^2}, \tag{6}$$

where G_o is the total surface density of gA in the bilayer and G_2 is the dimer surface density. Since only the dimeric peptides form an active channel, G_2 was determined electrically by using the mean single-channel conductance

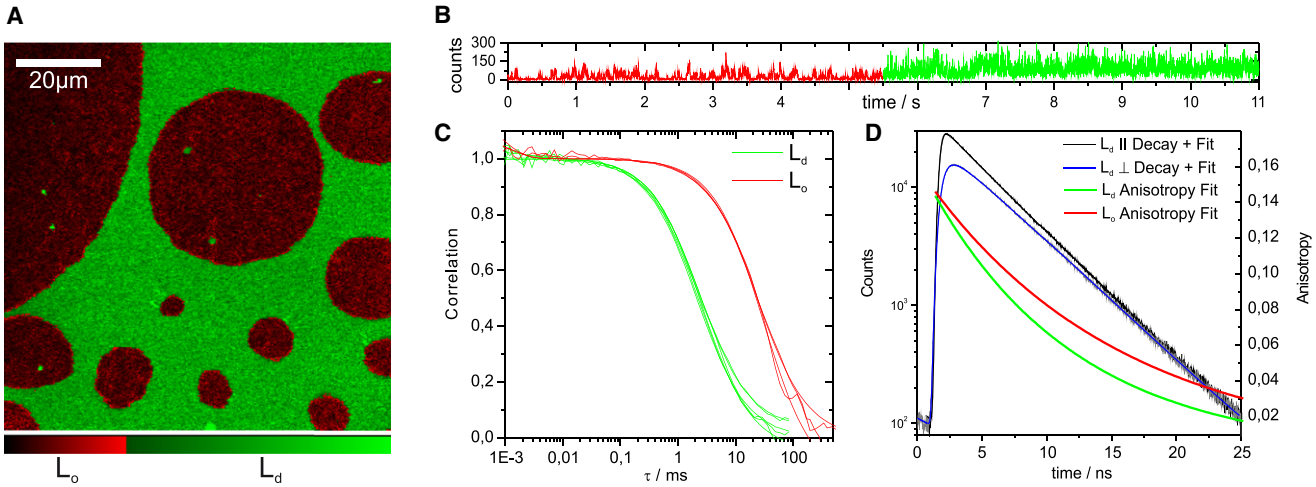

FIGURE 2 Lateral and rotational mobility in DOPC/DSPC/CO (2:1:1) bilayers at 23°C. (*A*) Intensity image of a phase-separated membrane (*xy* plane). A look-up table was used to emphasize the partitioning of the probe DPPE647 (*green*, L_d; *red*, L_o). (*B*) Fluctuating photon-count time trace binned at 1-ms resolution from a single point measurement in the membrane plane. Due to the fluid nature of the system, both phases crossed the confocal volume, revealed by the jump in count rate at ~5.5 s. (*C*) FCS data obtained from fluctuations in the L_d and L_o phases. The correlation curve is shifted to longer times for L_o, indicating the decrease in mobility. (*D*) Fluorescence intensity decay for parallel and perpendicular polarized emission after pulsed excitation of DPPE647 in the L_d phase. The fits yield the lifetime and the rotational correlation time of the probe. The anisotropy decay is slower in the L_o phase, indicating a lowered rotational mobility. The resulting lateral and rotational diffusion coefficients are listed in Tables 1 and 2.

to calculate the number of open channels from the total current amplitude. G_2 was divided by the total surface area of the bilayer, which was determined from laser scanning images. G_o was determined by FCS. The surface density of the fluorescent gA was directly calculated from the number of particles and the waist radius of the confocal spot. G_o was corrected by the degree of labeling.

RESULTS

Phase separation

Horizontal bilayers made of DOPC/DSPC/CO (2:1:1) exhibited large-scale phase separation into L_d and L_o domains at room temperature (Fig. 2 *A*). Segregated domains had a circular shape and were highly dynamic, i.e., they showed fusion to larger, also circular, domains (see Movie S1 in the Supporting Material). This is in agreement with the phase behavior of ternary lipid bilayers reported elsewhere (37) and indicates that both phases were in a fluidlike state. Domain formation was visualized by fluorescence emission of Atto647N-lipids phosphoethanolamine (DPPE647), sphingomyelin (SM647), and ceramide (CER647). All of the labeled lipids showed a similar partitioning pattern (Fig. 2 *A*). The bright regions were identified as the L_d phase by colocalization of fluorescently labeled cholesterol (CO-BDY), which has been shown to preferentially partition into the L_d phase (25). CO-BDY had a partitioning coefficient at 23°C (L_o/L_d) of $\gamma = 0.26$ which is similar to the distribution of this probe in solvent-free bilayers (25). In contrast to native SM and CER, the Atto647N-labeled lipids partitioned predominantly in the L_d phase. The partitioning coefficient was $\gamma \approx 0.1$ for CER647, SM647, and DPPE647 (Table 1). However, this effect has been observed for the majority of other lipid-dye combinations as well. The native partitioning of lipids has been found to be disturbed after labeling with a photostable, but bulky fluorophore (45,46). Nevertheless, these fluorescent sphingolipid analogs (SM647, CER647) have been found to form transient molecular complexes in the plasma membranes of living cells independent of the dye position or even the nature of the headgroup (11).

Lateral mobility of lipid probes in the L_o and L_d phases

Next, we compare the mobility of lipids in the L_d and L_o phases. For an exact determination of the diffusion coefficients, we applied *z*-scan FCS (42). The focus was moved incrementally in the z-direction through the bilayer plane. The correlation data and the corresponding diffusion times, $\tau_D(\Delta z)$, were determined (Eq. 3) for the different *z*-positions, Δz. The dependence of τ_D on Δz allowed for an exact determination of the lateral diffusion coefficients (Eq. 4). First, we checked the lateral mobility of DPPE647, SM647, and CER647 in DOPC, i.e., in pure L_d-phase bilayers at 23°C. All probes had comparable mobilities in the range $D_{lat} \approx$ 20–24 $\mu m^2/s$ (Table 1). Upon addition of 20 mol % cholesterol to the DOPC bilayer, lateral mobilities of the probes

TABLE 1 Lateral diffusion coefficients and partitioning of lipid probes in the L_o and L_d phases

Probe	L_o ($\mu m^2/s$)	L_d ($\mu m^2/s$)	c (L_o)/c (L_d)
CO-BDY	3.6 ± 0.1	25.6 ± 2.9	0.26 ± 0.08
DPPE647	2.0 ± 0.4	24.3 ± 2.4	0.10 ± 0.01
SM647	2.7 ± 0.5	18.4 ± 2.1	0.11 ± 0.07
CER647	3.2 ± 0.5	18.9 ± 3.9	0.07 ± 0.04

did not change significantly (data not shown). In other studies, lipid diffusion in the L_d phase was found to be slightly decreased upon addition of 20 mol % cholesterol (13). In case of domain formation in the ternary lipid mixtures (DOPC/DSPC/CO, 2:1:1) (Fig. 2 *A*), the recorded photon traces were used to differentiate between mobility in bright (L_d) and dark (L_o) domains (Fig. 2 *B*). Because the lateral diffusion in the L_d domains ($D_{lat} \approx$ 18–25 $\mu m^2/s$) (Table 1) was similar to that determined for the pure DOPC L_d-phase bilayers, we can conclude that the additional saturated lipid DSPC mostly partitioned in the L_o phase at 23°C. In contrast, diffusion in the L_o domains was 7- to 12-fold slower ($D_{lat} \approx$ 2–3 $\mu m^2/s$) (Fig. 2 *C* and Table 1).

Rotational diffusion in the L_d and L_o phases

We utilized the same photon traces that were the basis of the FCS analysis for the TRA analysis. The time-resolved fluorescence decays recorded for parallel and perpendicular polarization (Fig. 2 *D*) were analyzed (Eqs. 1 and 2) to obtain the rotational diffusion coefficient, D_{rot}, and the fluorescence lifetime, τ_{FL}, of the fluorescent lipid analogs CER647, SM647, and DPPE647 in both phases. A single anisotropic decay component and a single fluorescence lifetime were sufficient to yield statistically reliable fits. In pure DOPC (L_d) membranes, the rotational diffusion coefficient was $D_{rot} \approx 2.4 \times 10^7\ s^{-1}$ for all three lipids (Table 2). This value is in the same range as rotational diffusion coefficients of comparable lipid probes in an L_d membrane measured with single-molecule anisotropy imaging (47). Under phase-separating conditions, lipid rotation occurred at $D_{rot} \approx 1.4 \times 10^7\ s^{-1}$ in the L_d phase and between $D_{rot} \approx 1.0 \times 10^7\ s^{-1}$ and $D_{rot} \approx 0.8 \times 10^7\ s^{-1}$ in the L_o phase (Table 2). The decreased rotational mobility in the L_o domains is in line with the characteristic higher lipid order and a condensed packing in the L_o phase. The reduced rotational motion in the L_d phase under phase-separating conditions compared to that for pure L_d bilayers indicates also that the L_d phase changes its microviscosity. However, this change does not significantly affect the lateral diffusion constant (see above). Since addition of 20 mol % cholesterol to a pure L_d bilayer does not change the rotational motion (data not shown) of the lipid probes, we have to conclude that residual amounts of DSPC are present in the L_d phase under phase-separating conditions.

Steady-state anisotropy

To visualize the steady-state anisotropy in the bilayer, we calculated anisotropy images pixel by pixel from the signal intensity in the parallel and perpendicular detection channels (Eq. 5). Fig. 3 shows the intensity and the anisotropy image of a DOPC/DSPC/CO mixture at 23°C. As before (Fig. 2 *A*), the partitioning of the probe is evident in the intensity image (Fig. 3 *A*), where the dark domains correspond to the L_o phase. The anisotropy image (Fig. 3 *B*) depicts slightly larger anisotropy values in the L_o phase,

TABLE 2 Rotational correlation time (Φ), initial anisotropy (β), and fluorescence lifetime (τ_{FL}) of lipid probes in the L_o and L_d phases

	L_o		L_d		
Probe	Φ (ns)	β	Φ (ns)	β	τ_{FL} (ns)
DPPE647	16.5 ± 1.3	0.15	12.1 ± 0.2	0.15	4.1
SM647	20.3 ± 2.3	0.11	13.2 ± 2.0	0.14	4.1
CER647	21.5 ± 1.3	0.12	9.2 ± 0.2	0.12	4.0

which is in line with a decreased rotational diffusion coefficient. However, in contrast to the L_d phase, where the values are narrowly distributed around 0.1, a wide range of anisotropy values becomes obvious for the L_o phase, ranging from ~0.1 to 0.3–0.4, with the higher values indicating very slow rotational motion. To get further insight into this strong inhomogeneity, we recorded steady-state anisotropy values at the single-molecule level.

To determine the steady-state anisotropy from single molecules, we positioned the laser spot on different positions in the L_d and L_o phases of the bilayer and recorded photon traces over time. The concentration of DPPE647 was reduced such that less than one fluorescent molecule was present per laser spot per time. The fluorescence bursts indicating single-molecule transits (Fig. 3 *C*) were used

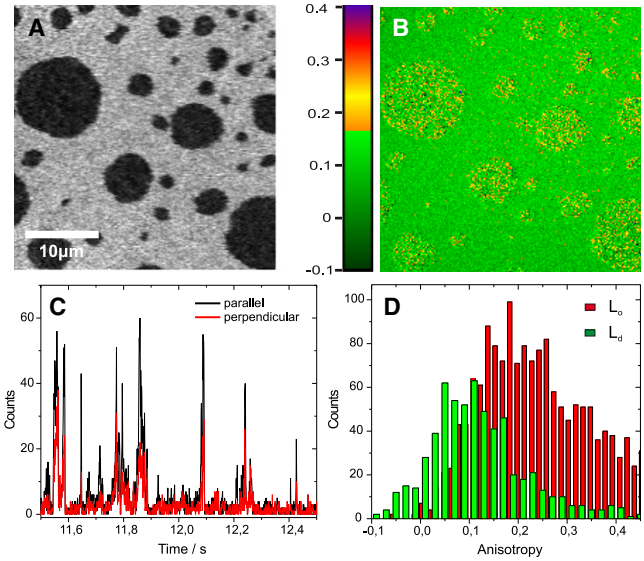

FIGURE 3 Steady-state anisotropy and FCS diffusion laws in DOPC/DSPC/CO (2:1:1) bilayers, for probe DPPE647. (*A*) Intensity image of a bilayer with L_o (*dark*) and L_d (*bright*) domains. (*B*) Pixel-by-pixel calculated anisotropy from parallel and perpendicular images. The anisotropy was higher and more heterogeneous in the L_o domains. (*C*) Section of a photon trace recorded by a point measurement in the L_o phase (1-ms binning). Single-molecule transits are visible as photon bursts. For each transit, the anisotropy was calculated by burst integration of the parallel and perpendicular detection channels and application of Eq. 5. (*D*) Single-molecule anisotropy histograms in the L_d and L_o phases of the membrane, with peaks at ~0.1 and 0.16, respectively. The distribution in the L_o phase is shifted to higher anisotropy values and is much broader, confirming the lowered rotational mobility and indicating a heterogeneous lipid environment in the L_o phase.

to calculate the steady-state anisotropy (Eq. 5). Selection of >2000 single-molecule fluorescence bursts resulted in a histogram of anisotropy values for the L_d and L_o phase (Fig. 3 *D*). The distribution of anisotropy values of the L_o phase peaks at much higher values ($\bar{r} \approx 0.16$) and is much broader than the distribution of values of the L_d phase ($\bar{r} \approx 0.1$), tailing off to very high values $\bar{r} > 0.3$, confirming the heterogeneity in anisotropy previously observed using anisotropy imaging. It seems that the L_o phase itself contains a subpopulation in which lipid rotation is significantly reduced. Unfortunately, the ability to resolve additional, very slow rotational components in the L_o phase is limited by the fluorescence lifetime (4 ns) of the lipid analog. Thus, the resolution of our time-resolved anisotropy data was not good enough to reliably determine very slow rotational components.

Partitioning and electrophysiological activity of gramicidin A in lipid domains

The short antibiotic peptide gA is one of the best characterized ion channels to date (38,48). It is able to form a 2.8-nm-long transmembrane β-helix with an aqueous pore diameter of 0.4 nm. This cation-conducting conformation was found to be the result of an N- to N-terminal dimerization of two gA monomers (44). The structure of the transmembrane gA dimer itself seems to be unaffected by the lipid composition of the membrane (49,50). However, the dimerization constant is dependent on the hydrophobic thickness and lipid composition of the bilayer, as well as the membrane potential (44,48,51).

Here, we used a functional, C-terminal, Atto637-labeled derivate of gA to study the effect of liquid-liquid phase separation on the activity and partitioning of gA. The peptide was added directly to the lipid solution (DOPC/DSPC/CO, 1:1:1) in a molar ratio of 1:10000. The bilayer was prepared at 39°C to ensure a homogeneous mixing of lipid species (Fig. 4 *A*). The gA concentration in the membrane was determined by FCS (Fig. 4 *C*), and the active dimer concentration was determined by electrical conductance measurements (Fig. 4 *B*). As the membrane was cooled to 23°C, large-scale L_o domains segregated from the L_d phase. gA was found to be largely excluded from the L_o domains (Fig. 4 *A*). Simultaneously, the number of electrically active dimers increased 3.3-fold as the lipids phase-separated. Accordingly, the surface density of gA in the L_d phase, determined by FCS, increased 2.2-fold at 23°C. It is interesting that the dimerization constant, *K* (Eq. 6), did not change significantly between

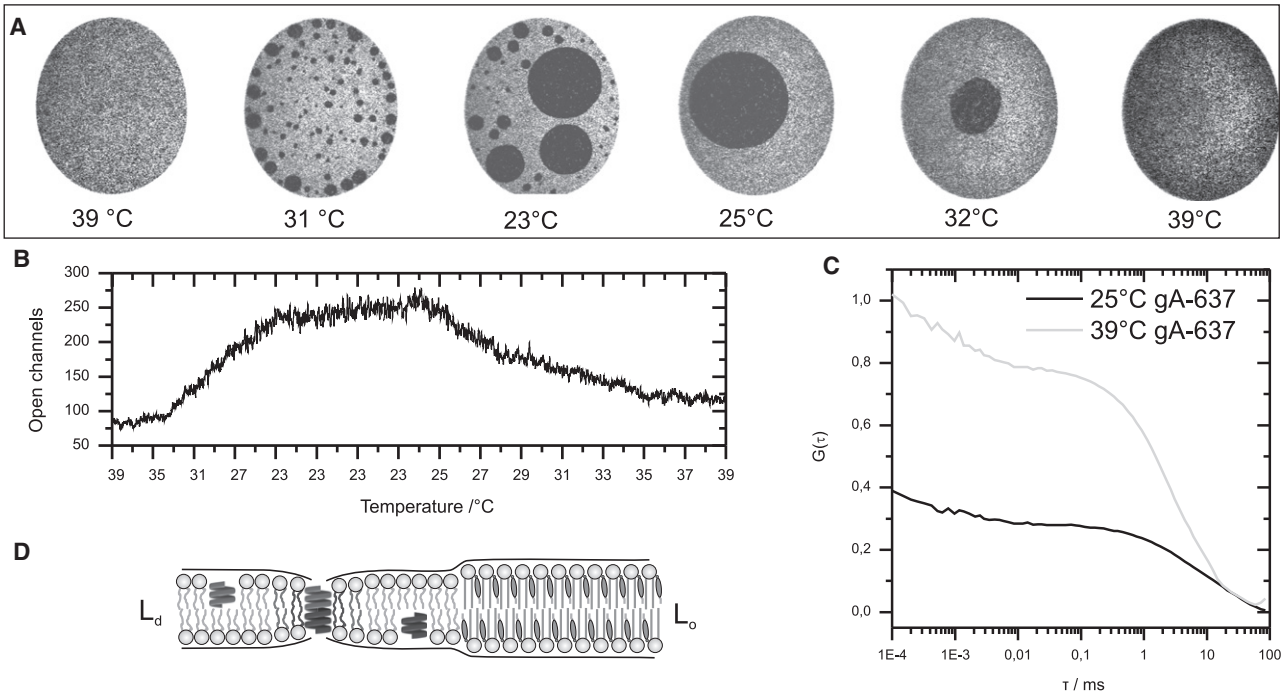

FIGURE 4 Phase partitioning and electrical activity of gramicidin A. (*A*) Lipid phase separation in a DOPC/DSPC/CO (1:1:1) membrane (Ø = 100 μm) containing gA-637 was induced by cooling the bilayer from 39°C to 23°C. gA-637 was largely excluded from the L_o domains (*dark*). (*B*) Simultaneous recording of the electrical activity of gA-637 monitored via conductance measurements of the bilayer. The number of open gA channels increased 3.3-fold as the lipids phase-separated. (*C*) FCS measurements at 39°C and 23°C revealed that the surface density in the L_d phase at 23°C was increased 2.2-fold compared to the homogenous membrane at 39°C. The dimerization constant determined by FCS from the number of open channels and the total number of gA-637 changed during phase separation from $K_{39°C} = 3.3 \times 10^{11}$ cm^2/mol to $K_{23°C} = 4.1 \times 10^{11}$ cm^2/mol. (*D*) Scheme of gA monomers forming an active dimer in the L_d phase. The peptide is energetically excluded from the thicker and ordered cholesterol-enriched L_o phase. The thinner membrane in the L_d phase results in a higher dimerization constant of gA. However, the increased electrical activity of gA in the L_d phase can be mainly attributed to the increased surface density due to exclusion from the L_o domains.

39°C and 23°C, with values of 3.3×10^{11} cm^2/mol at 39°C and 4.1×10^{11} cm^2/mol at 23°C. Thus, the increased electrical activity at 23°C was mainly caused by the higher surface density of gA due to exclusion from the L_o domains, and not by a change of hydrophobic thickness of the membrane. When the temperature was returned to 39°C, lipid domains mixed again to a single phase. As expected, the number of active gA dimers decreased again. The results show that the electrophysiological activity of gA can be simply regulated by phase partitioning in lipid domains.

DISCUSSION

The aim of this study was to characterize the diffusion and electrical properties of horizontal black lipid bilayers containing biological relevant ternary lipid mixtures and to compare the results with other established membrane model systems. In addition, the potential of the setup to relate the electrical activity of ion channels to partitioning behavior in lipid domains was explored using the ion channel gA.

In contrast to supported bilayers or giant unilamellar vesicles, for any black lipid membrane preparation the use of a hydrocarbon solvent is essential, because the actual bilayer is thinned out from the bulk region of a solvent-lipid mixture (Torus). This raises the problem that the solvent may also partition inside the actual bilayer, which may cause changes in the natural properties of the membrane. To address this, we tested the influence of three different solvents on lipid diffusion (Fig. S1 in the Supporting Material). Our results show that the lateral and rotational diffusion constants depend on the nature of the hydrocarbon solvents used for bilayer preparation. Since the lateral and rotational mobility increased with decreasing chain length of the solvents, we can conclude that shorter alkanes (<16 carbon atoms) partially reside in the bilayer membrane after equilibration of the horizontal bilayer system. This causes a more fluid membrane and a depressed T_m compared to solvent-free bilayers. In other studies on BLMs, solvent partitioning was also found to increase the bilayer thickness, probably by intercalation of the solvent molecules between the inner and outer leaflets (34,52,53). However, in our measurements on phase separation in ternary lipid bilayers, domain formation always extended through both leaflets of the membrane, regardless of the solvent used (Fig. 2 *A*). Thus, the coupling between the opposing leaflets is not affected by the presence of decane, hexane, or squalene.

Apart from solvent-partitioning effects, large-scale domain segregation in ternary horizontal bilayers occurred in accordance with the established phase diagrams, which were derived using giant unilamellar vesicles (18–21). Moreover, the basic characteristics of liquid-liquid domain formation can be reconstituted in horizontal bilayers: lateral and rotational diffusion is significantly reduced, and the lipid order is higher in the L_o domains compared to the L_d domains. We found an approximately eightfold decrease in lateral diffusion (L_d/L_o). Similar differences between lateral diffusion in L_o and L_d domains of 3- to 20-fold have been reported for other model membranes (12,25,54).

A detailed analysis of lipid anisotropy, which reports the very local environment of the probe, and of the lateral diffusion on various lengthscales revealed that the anisotropy is homogeneous and lateral diffusion is free in the L_d phase. It is of interest that both the anisotropy values and the lateral diffusion law (Fig. S2) indicate a heterogeneous lipid distribution in the L_o phase at 23°C. The origin of the heterogeneities is not clear, but they could be due to a nonideal segregation of the lipid species such that nano-L_d domains remain in the L_o phase. Another possibility may be the formation of nano-S_o domains in regions of the L_o phase where cholesterol content is low. Further details on potential nanodomains in the L_o phase may be gathered by combining FCS (or TRA) and stimulated emission depletion nanoscopy (55), a microscopy approach featuring a spatial resolution far below that of conventional microscopy, i.e., in the range of the nanodomain sizes (11,56).

To explore the full potential of the horizontal bilayer technique, we studied the influence of lipid phase partitioning on the electrophysiological activity of the ion channel gA. As a control we used protein-free ternary lipid bilayers that were cooled below the phase transition temperature (Fig. S3). Our results show that ternary lipid bilayers remain electrically sealed at the transition from the L_o to the L_d phase, which is a requirement for electrophysiological measurement of ion channels. The results from the gA experiments show that the monomeric as well as the dimeric gA are largely excluded from the L_o phase. The sorting of the peptide to the L_d phase resulted in an increased electrophysiological activity, which was monitored by an increase in detected membrane current. The activity of gA was found to be simply modulated by the surface density in the lipid domains. This is consistent with the results of Boheim et al. (57), who found indications for lipid domain partitioning effects of gA and alamethicin: Near the transition temperature of steroyl-myristoyl-phosphatidylcholine bilayers the electrical activity of the peptides was significantly amplified. However, in that study, the setup allowed only for electrical recordings. Thus, the authors could only speculate about domain-partitioning effects of the peptides. In this study, we could directly relate the sorting of gA due to phase partitioning to its electrophysiological activity. Our results show that the setup presented here can be used to study quantitatively the relation of ion channel function and lipid phase separation in a defined system. The technique could now be applied to more complex proteins that are thought to be regulated by lipid domains (48,58).

SUPPORTING MATERIAL

Three figures and one movie are available at http://www.biophysj.org/biophysj/supplemental/S0006-3495(10)00366-8.

Technical assistance from Birgit Hemmis is gratefully acknowledged.

This work was financially supported by grants from the Deutsche Forschungsgemeinschaft (SFB 431) and the Bundesministerium fuer Bildung und Forschung (BMBF, FKZ: 0315010).

REFERENCES

1. Fielding, C. J., editor. 2005. Lipid Rafts and Caveolae. Wiley-VCH, Weinheim, Germany.
2. van Meer, G., D. R. Voelker, and G. W. Feigenson. 2008. Membrane lipids: where they are and how they behave. *Nat. Rev. Mol. Cell Biol.* 9:112–124.
3. Simons, K., and G. van Meer. 1988. Lipid sorting in epithelial cells. *Biochemistry*. 27:6197–6202.
4. Sako, Y., and A. Kusumi. 1994. Compartmentalized structure of the plasma membrane for receptor movements as revealed by a nanometer-level motion analysis. *J. Cell Biol.* 125:1251–1264.
5. Simons, K., and E. Ikonen. 1997. Functional rafts in cell membranes. *Nature*. 387:569–572.
6. Gaus, K., E. Gratton, …, W. Jessup. 2003. Visualizing lipid structure and raft domains in living cells with two-photon microscopy. *Proc. Natl. Acad. Sci. USA*. 100:15554–15559.
7. Wawrezinieck, L., H. Rigneault, …, P. F. Lenne. 2005. Fluorescence correlation spectroscopy diffusion laws to probe the submicron cell membrane organization. *Biophys. J*. 89:4029–4042.
8. Lenne, P.-F., L. Wawrezinieck, …, D. Marguet. 2006. Dynamic molecular confinement in the plasma membrane by microdomains and the cytoskeleton meshwork. *EMBO J*. 25:3245–3256.
9. Wenger, J., F. Conchonaud, …, P. F. Lenne. 2007. Diffusion analysis within single nanometric apertures reveals the ultrafine cell membrane organization. *Biophys. J*. 92:913–919.
10. Lingwood, D., J. Ries, …, K. Simons. 2008. Plasma membranes are poised for activation of raft phase coalescence at physiological temperature. *Proc. Natl. Acad. Sci. USA*. 105:10005–10010.
11. Eggeling, C., C. Ringemann, …, S. W. Hell. 2009. Direct observation of the nanoscale dynamics of membrane lipids in a living cell. *Nature*. 457:1159–1162.
12. Dietrich, C., L. A. Bagatolli, …, E. Gratton. 2001. Lipid rafts reconstituted in model membranes. *Biophys. J*. 80:1417–1428.
13. Scherfeld, D., N. Kahya, and P. Schwille. 2003. Lipid dynamics and domain formation in model membranes composed of ternary mixtures of unsaturated and saturated phosphatidylcholines and cholesterol. *Biophys. J*. 85:3758–3768.
14. Crane, J. M., and L. K. Tamm. 2004. Role of cholesterol in the formation and nature of lipid rafts in planar and spherical model membranes. *Biophys. J*. 86:2965–2979.
15. Kiessling, V., J. M. Crane, and L. K. Tamm. 2006. Transbilayer effects of raft-like lipid domains in asymmetric planar bilayers measured by single molecule tracking. *Biophys. J*. 91:3313–3326.
16. Baumgart, T., A. T. Hammond, …, W. W. Webb. 2007. Large-scale fluid/fluid phase separation of proteins and lipids in giant plasma membrane vesicles. *Proc. Natl. Acad. Sci. USA*. 104:3165–3170.
17. Feigenson, G. W. 2007. Phase boundaries and biological membranes. *Annu. Rev. Biophys. Biomol. Struct*. 36:63–77.
18. Feigenson, G. W., and J. T. Buboltz. 2001. Ternary phase diagram of dipalmitoyl-PC/dilauroyl-PC/cholesterol: nanoscopic domain formation driven by cholesterol. *Biophys. J*. 80:2775–2788.
19. de Almeida, R. F. M., A. Fedorov, and M. Prieto. 2003. Sphingomyelin/phosphatidylcholine/cholesterol phase diagram: boundaries and composition of lipid rafts. *Biophys. J*. 85:2406–2416.
20. Feigenson, G. W. 2006. Phase behavior of lipid mixtures. *Nat. Chem. Biol*. 2:560–563.
21. Goñi, F. M., A. Alonso, …, J. L. Thewalt. 2008. Phase diagrams of lipid mixtures relevant to the study of membrane rafts. *Biochim. Biophys. Acta*. 1781:665–684.
22. Magde, D., E. Elson, and W. W. Webb. 1972. Thermodynamic fluctuations in a reacting system–measurement by fluorescence correlation spectroscopy. *Phys. Rev. Lett*. 29:705–708.
23. Chiantia, S., J. Ries, and P. Schwille. 2008. Fluorescence correlation spectroscopy in membrane structure elucidation. *Biochim. Biophys. Acta*. 1788:225–233.
24. Dertinger, T., V. Pacheco, …, J. Enderlein. 2007. Two-focus fluorescence correlation spectroscopy: a new tool for accurate and absolute diffusion measurements. *ChemPhysChem*. 8:433–443.
25. Ries, J., S. Chiantia, and P. Schwille. 2009. Accurate determination of membrane dynamics with line-scan FCS. *Biophys. J*. 96:1999–2008.
26. Jähnig, F. 1979. Structural order of lipids and proteins in membranes: evaluation of fluorescence anisotropy data. *Proc. Natl. Acad. Sci. USA*. 76:6361–6365.
27. Goswami, D., K. Gowrishankar, …, S. Mayor. 2008. Nanoclusters of GPI-anchored proteins are formed by cortical actin-driven activity. *Cell*. 135:1085–1097.
28. Gidwani, A., D. Holowka, and B. Baird. 2001. Fluorescence anisotropy measurements of lipid order in plasma membranes and lipid rafts from RBL-2H3 mast cells. *Biochemistry*. 40:12422–12429.
29. Ariola, F. S., Z. Li, …, A. A. Heikal. 2009. Membrane fluidity and lipid order in ternary giant unilamellar vesicles using a new bodipy-cholesterol derivative. *Biophys. J*. 96:2696–2708.
30. Hille, B. 2001. Ion Channels of Excitable Membranes. Sinauer Associates, Springfield, MA.
31. Mueller, P., and D. O. Rudin. 1963. Induced excitability in reconstituted cell membrane structure. *J. Theor. Biol*. 4:268–280.
32. Hladky, S. B., and D. A. Haydon. 1970. Discreteness of conductance change in bimolecular lipid membranes in the presence of certain antibiotics. *Nature*. 225:451–453.
33. Hill, K., K. Model, …, N. Pfanner. 1998. Tom40 forms the hydrophilic channel of the mitochondrial import pore for preproteins [see comment]. *Nature*. 395:516–521.
34. Fahey, P. F., D. E. Koppel, …, W. W. Webb. 1977. Lateral diffusion in planar lipid bilayers. *Science*. 195:305–306.
35. Ide, T., and T. Yanagida. 1999. An artificial lipid bilayer formed on an agarose-coated glass for simultaneous electrical and optical measurement of single ion channels. *Biochem. Biophys. Res. Commun*. 265:595–599.
36. Borisenko, V., T. Lougheed, …, G. J. Schütz. 2003. Simultaneous optical and electrical recording of single gramicidin channels. *Biophys. J*. 84:612–622.
37. Samsonov, A. V., I. Mihalyov, and F. S. Cohen. 2001. Characterization of cholesterol-sphingomyelin domains and their dynamics in bilayer membranes. *Biophys. J*. 81:1486–1500.
38. Andersen, O. S., R. E. Koeppe, 2nd, and B. Roux. 2005. Gramicidin channels. *IEEE Trans. Nanobioscience*. 4:10–20.
39. Eggeling, C., K. Gall, …, L. Brand. 2003. Confocal fluorescence techniques in industrial application. *Proc. SPIE*. 4692:101–109.
40. Widengren, J., U. Mets, and R. Rigler. 1995. Fluorescence correlation spectroscopy of triplet states in solution: a theoretical and experimental study. *J. Phys. Chem*. 99:13368–13379.
41. Müller, C. B., A. Loman, …, J. Enderlein. 2008. Precise measurement of diffusion by multi-color dual-focus fluorescence correlation spectroscopy. *Europhys. Lett*. 83:46001.
42. Benda, A., M. Bene, …, M. Hof. 2003. How to determine diffusion coefficients in planar phospholipid systems by confocal fluorescence correlation spectroscopy. *Langmuir*. 19:4120–4126.
43. Schaffer, J., A. Volkmer, …, C. A. M. Seidel. 1999. Identification of single molecules in aqueous solution by time-resolved fluorescence anisotropy. *J. Phys. Chem. A*. 103:331–336.
44. Veatch, W. R., R. Mathies, …, L. Stryer. 1975. Simultaneous fluorescence and conductance studies of planar bilayer membranes containing a highly active and fluorescent analog of gramicidin A. *J. Mol. Biol*. 99:75–92.

45. Baumgart, T., G. Hunt, …, G. W. Feigenson. 2007. Fluorescence probe partitioning between L_o/L_d phases in lipid membranes. *Biochim. Biophys. Acta*. 1768:2182–2194.

46. Shaw, J. E., R. F. Epand, …, C. M. Yip. 2006. Correlated fluorescence-atomic force microscopy of membrane domains: structure of fluorescence probes determines lipid localization. *Biophys. J*. 90:2170–2178.

47. Harms, G. S., M. Sonnleitner, …, T. Schmidt. 1999. Single-molecule anisotropy imaging. *Biophys. J*. 77:2864–2870.

48. Lundbaek, J. A., S. A. Collingwood, …, O. S. Andersen. 2010. Lipid bilayer regulation of membrane protein function: gramicidin channels as molecular force probes. *J. R. Soc. Interface*. 7:373–395.

49. Allen, T. W., O. S. Andersen, and B. Roux. 2003. Structure of gramicidin a in a lipid bilayer environment determined using molecular dynamics simulations and solid-state NMR data. *J. Am. Chem. Soc*. 125:9868–9877.

50. Ketchem, R., B. Roux, and T. Cross. 1997. High-resolution polypeptide structure in a lamellar phase lipid environment from solid state NMR derived orientational constraints. *Structure*. 5:1655–1669.

51. Sandblom, J., J. Galvanovskis, and B. Jilderos. 2001. Voltage-dependent formation of gramicidin channels in lipid bilayers. *Biophys. J*. 81:827–837.

52. White, S. H., and T. E. Thompson. 1973. Capacitance, area, and thickness variation in thin lipid films. *Biochim. Biophys. Acta*. 323:7–22.

53. White, S. H. 1976. The lipid bilayer as a ''solvent'' for small hydrophobic molecules. *Nature*. 262:421–422.

54. Bacia, K., D. Scherfeld, …, P. Schwille. 2004. Fluorescence correlation spectroscopy relates rafts in model and native membranes. *Biophys. J*. 87:1034–1043.

55. Hell, S. W., and J. Wichmann. 1994. Breaking the diffraction resolution limit by stimulated emission: stimulated-emission-depletion fluorescence microscopy. *Opt. Lett*. 19:780–782.

56. Ringemann, C., B. Harke, …, C. Eggeling. 2009. Exploring single-molecule dynamics with fluorescence nanoscopy. *N. J. Phys*. 11:103054.

57. Boheim, G., W. Hanke, and H. Eibl. 1980. Lipid phase transition in planar bilayer membrane and its effect on carrier- and pore-mediated ion transport. *Proc. Natl. Acad. Sci. USA*. 77:3403–3407.

58. Martens, J. R., K. O'Connell, and M. Tamkun. 2004. Targeting of ion channels to membrane microdomains: localization of KV channels to lipid rafts. *Trends Pharmacol. Sci*. 25:16–21.